Features of Reduction and Chemisorption Properties of Nanosized Iron(III) Oxide

A. S. Lyadov*, A. A. Kochubeev, E. B. Markova, O. P. Parenago, and S. N. Khadzhiev

Topchiev Institute of Petrochemical Synthesis, Russian Academy of Sciences, Moscow, Russia

*e-mail: lyadov@ips.ac.ru

Received April 21, 2016

Abstract—Nanosized iron(III) oxide with an average particle size of 8–10 nm has been synthesized by the thermolysis of iron(III) acetylacetonate using diphenyl ether as a dispersion medium. Reduction processes in a hydrogen atmosphere in the presence of nanosized iron oxide and natural mineral hematite (Fe_2O_3) have been studied by the temperature-programmed reduction method. The activation energies of the reduction processes have been determined by the Kissinger method; it has been shown that, in the case of nano-Fe_2O_3, the activation energies are several times higher than the respective values observed for hematite. The adsorption properties of nano-Fe_2O_3 and hematite have been studied; the isosteric heats of chemisorption of hydrogen and carbon monoxide on the surface of these samples have been determined.

The unique magnetic, optical, catalytic, and electrochemical properties of nanosized iron(III) oxide (Fe_2O_3) are commonly use in practice [1]. The introduction of nanosized iron oxide into biological objects makes it possible to solve a number of biomedical problems, such as the design of contrast agents for MRI diagnosis, targeted drug delivery, immunoassays and separation of cell material, and effective detoxication. The biomedical and bioengineering application of nanosized Fe_2O_3 owes its existence not only to the unique magnetic and optical properties, but also to an extremely low toxicity and high biocompatibility of this compound [2].

Another field of application of nanosized Fe_2O_3 is catalysis and photocatalysis. A large number of publications have been focused on the use of nano-Fe_2O_3 as a catalyst in the conversion of synthesis gas to hydrocarbons (Fischer–Tropsch synthesis) [3]. In addition, the prospects for the use of this catalyst in the desulfurization of crude oil and petroleum fractions have been reported. An ingenious method for the production of synthetic hydrocarbons under conditions of a three-phase Fischer–Tropsch process in the presence of an iron-containing nanocatalyst placed in the dispersion medium has been developed [4, 5]. In this case, the extremely high activity of the nanoparticles provides the catalyst productivity that is several times higher than the productivity of commercial catalysts.

The use of nano-Fe_2O_3 as a catalyst requires the reduction of this material [6]; therefore, it is relevant to study the reducing ability of iron oxides. Another important issue is examination of the chemisorption of hydrogen and carbon monoxide on the surface of nanoparticles. Results of the studies will contribute to the development of concepts concerning Fischer–Tropsch synthesis and some other catalytic processes under conditions of nanoheterogeneous catalysis and in the case of using nano-Fe_2O_3 as an indicator in gas detectors.

The aim of this study was to examine the features of reduction of nanosized iron(III) oxide with an average particle size of 8–10 nm by temperature-programmed reduction (TPR) and the chemisorption of hydrogen and carbon monoxide on the nano-Fe_2O_3 surface.

EXPERIMENTAL

Nanosized Fe_2O_3 was synthesized by the thermolysis of an iron-containing precursor in a dispersion medium. Iron acetylacetonate prepared as described in [7] was used as a precursor; the dispersion medium was diphenyl ether (DPE). The choice of DPE was based on the thermal stability, high boiling point (259°C), and low toxicity of this material. Iron acetylacetonate (0.5 g) was dissolved in 10 mL of DPE; 40 mL of DPE in a two-necked round-bottom flask equipped with a reflux condenser was heated in an oil bath to 200°C under vigorous stirring with a magnetic stirrer. After that, using a syringe, the iron acetylacetonate solution was rapidly introduced into hot DPE.

The resulting mixture was held under vigorous stirring for 2 h to provide the completion of thermolysis and the formation of iron oxide particles; after that, the mixture was cooled and analyzed. To study the features of reduction of Fe_2O_3 and the chemisorption processes involving it, DPE was removed by vacuum distillation; the resulting material was a black powder.

X-ray powder diffraction analysis was conducted on a Rigaku Ultima IV X-ray diffractometer equipped with a theta–theta goniometer using CoK_α radiation at a scan pitch of 0.02°, an exposure time of 1 s, and an angle measurement range of $2\theta = 10°–100°$. The X-ray diffraction patterns of the resulting compounds were indexed by homology using the data of the ICDD PDF-4 international database.

The particle size and morphology were determined by transmission electron microscopy (TEM) on a 120-kV Tecnai Spirit microscope. For analysis, the sample was dispersed in methanol by sonication and then deposited on a copper substrate.

The features of reduction of Fe_2O_3 were studied by TPR on a Micromeritics Auto Chem II instrument. The sample was placed in a quartz U-shaped reactor equipped with a thermocouple and then heated in a stream of a gas mixture (5 vol % hydrogen in argon) to a temperature of 1223 K. The feed rate of the gas mixture was 50 mL/min; the heating rate was 0.083, 0.167, and 0.333 K/s; the temperature inside the reactor was measured (thermocouple was placed at a distance of 5 mm from the sample surface); the absorption of the reducing agent was registered using a thermal conductivity detector.

The activation energy of the reduction processes was calculated by the Kissinger method [8] using the TPR data obtained at different heating rates of the samples from the slope of straight lines plotted in the Arrhenius coordinates $-\ln(b/T_{max}^2)-10^3/T_{max}$, where b is the heating rate of the sample (K/s) and T_{max} is the temperature of the absorption peak maximum of the reducing agent.

The chemisorption of carbon monoxide and hydrogen was studied in a U-shaped reactor using a Micromeritics ASAP 2020 instrument. Before measuring chemisorption, all samples were evacuated (10^{-6} mmHg) for 2 h. Chemisorption isotherms were recorded by measuring the absorption of hydrogen or carbon monoxide by the sample as a function of pressure at a constant temperature. The temperatures used in the studies were as follows: 50, 100, 150, 200, 220, 240, 260, 280, and 300°C. The choice of these values was based on the activity of iron-containing catalysts in this temperature range in Fischer–Tropsch synthesis. Quantitative measurements of the chemisorption parameters were conducted in a pressure range of 100–650 mmHg. Pressure was raised in steps of 50 mmHg.

On the basis of these data, using the van't Hoff equation, the enthalpies of chemisorption of hydrogen and carbon monoxide were calculated. To find the isosteric enthalpy values, it is necessary to determine the pressures at different temperatures for the chemisorption of the same amount of the gas using the experimental data and then to determine the isosteric enthalpy of chemisorption from the $\ln P - 1000/T$ plot.

RESULTS AND DISCUSSION

Nanosized iron oxide with an average particle size of 8–10 nm was prepared by the thermolysis of $Fe(AcAc)_3$ in DPE (Fig. 1a). For the black powder formed after the removal of DPE by vacuum distillation, TEM images were recorded (Fig. 1b).

According to expectations, the removal of the dispersion medium leads to the agglomeration of the nanoparticles; however, the original morphology and average size of the particles remain the same; thus, it can be assumed that this sample represents, to a certain extent, the properties of individual Fe_2O_3 nanoparticles.

The resulting sample was analyzed by TPR to study the reduction processes that occur in nanosized iron oxide during temperature rise in a reducing atmosphere. The TPV-profile of nano-Fe_2O_3 (Fig. 2a) is characterized by three well-shaped peaks that can be attributed to the following reduction processes [9]: nano-$Fe_2O_3 \rightarrow Fe_3O_4$ (peak 1); $Fe_3O_4 \rightarrow FeO$ (peak 2); and $FeO \rightarrow Fe$ (peak 3). For comparison, the TPR profile of hematite Fe_2O_3 was recorded (Fig. 2b); it exhibits only two peaks: the first peak corresponds to the reduction of hematite (Fe_2O_3) to magnetite (Fe_3O_4), while the second peak characterizes the conversion of magnetite to metallic iron. It should be noted that the reduction of hematite begins and proceeds at lower temperatures than the reduction of nano-Fe_2O_3. This difference can be explained not only by the size factor, but also by the initial phase composition of the two samples.

Figure 3 shows X-ray diffraction patterns of these samples. Nano-Fe_2O_3 crystallizes in the cubic crystal system (Fig. 3a), while hematite has a rhombohedral structure (Fig. 3b).

The TPR method not only provides information about the processes that occur in a substance during reduction, but also make it possible to determine the kinetic reduction parameters [10]. The activation energies of the reduction processes were determined by the Kissinger method. Table 1 shows the data for these calculations.

It should be noted that the activation energies of the reduction of nano-Fe_2O_3 are several times higher than the respective values of the reduction processes observed for hematite.
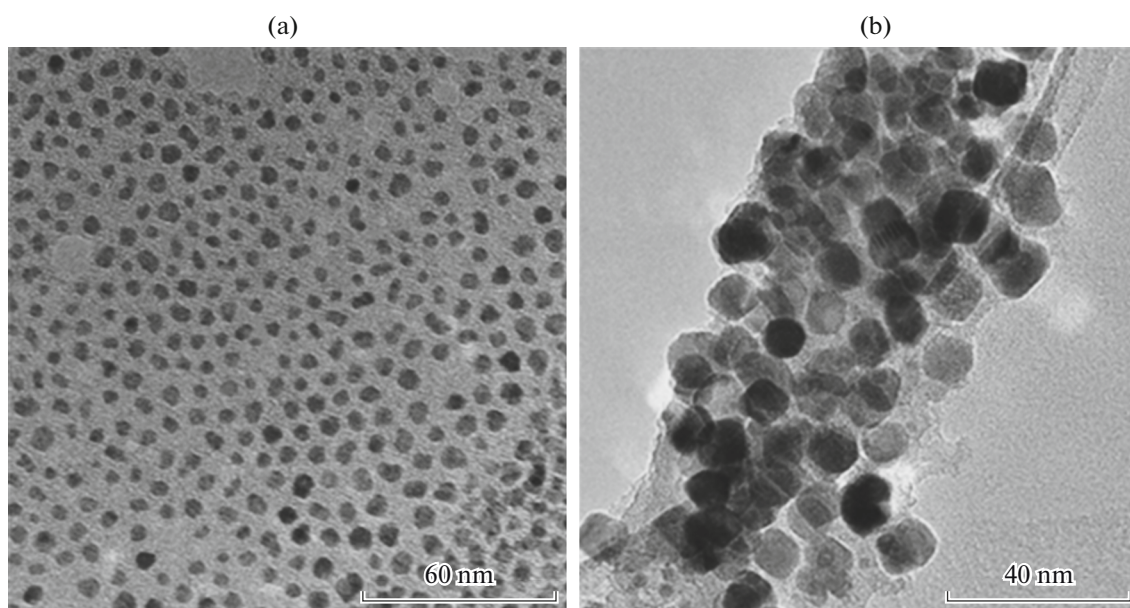
(a)

(b)

Fig. 1. TEM images of nanosized iron(III) oxide: (a) in the DPE medium and (b) after the removal of DPE.
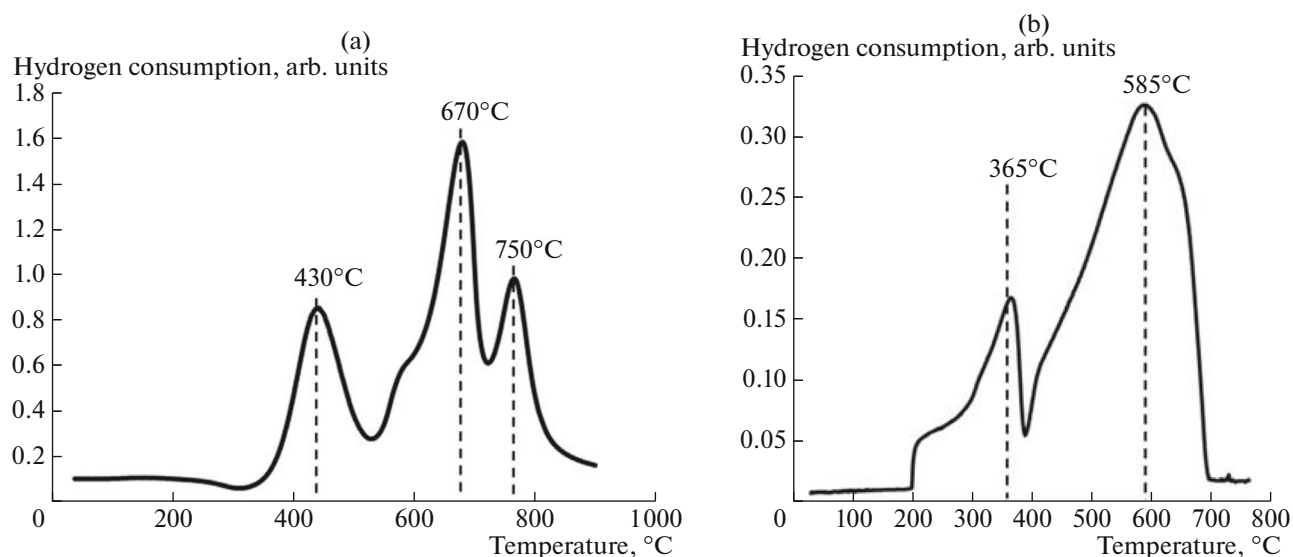

Fig. 2. TPR profiles of (a) nano-Fe_2O_3 and (b) hematite Fe_2O_3.

The chemisorption of carbon monoxide and hydrogen on the surface of nano-Fe_2O_3 and hematite was studied (Figs. 4a–4d). In the case of chemisorption of hydrogen, for both types of iron oxide, the amount of hydrogen chemisorbed on the sample surface increases with increasing temperature; however, the shapes of the isotherms are different. In the case of hematite, the adsorption isotherms correspond to type II or III according to the classification of Brunauer, Demming, Demming, and Teller (BDDT); this finding indicates the formation of a multilayer on the surface. The isotherms of nanosized iron oxide are, most probably, type I Langmuir isotherms according to the BDDT classification. These isotherms can be described in terms of the monolayer theory and, accordingly, by the Langmuir equation in an asymptotic approximation of the amount of adsorbed gas to the monolayer capacity. In this case, an increase in temperature leads to a shift of adsorption to the Henry region.

Differences in the behavior of hydrogen are more clearly shown by the chemisorption isobars (Fig. 5). The hydrogen chemisorption magnitude for the nano-
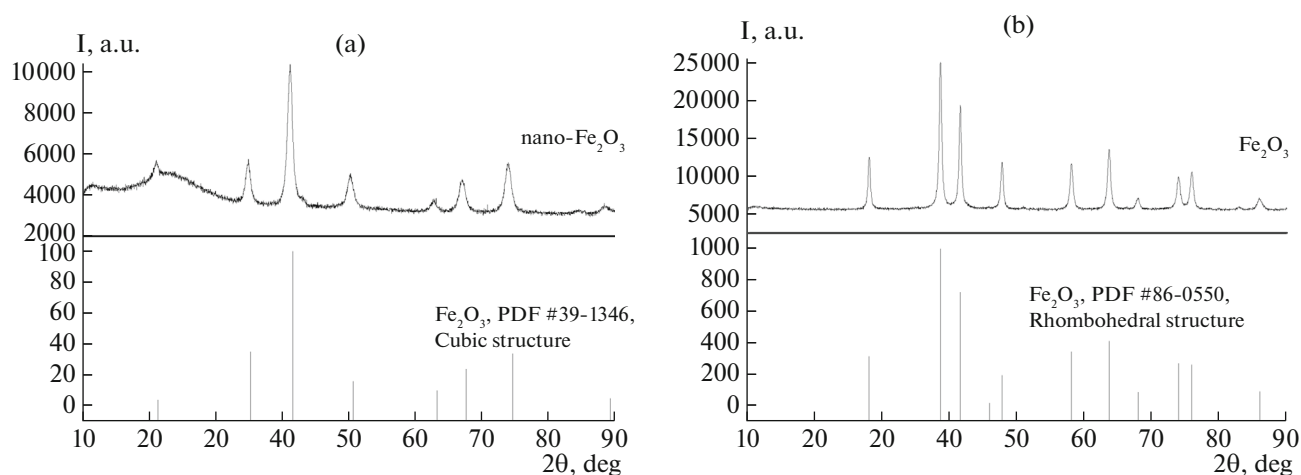
Fig. 3. X-ray diffraction patterns of (a) nano-Fe_2O_3 and (b) hematite Fe_2O_3.

sized sample at 300°C is 6 times higher than the chemisorption on the hematite surface.

In the case of CO chemisorption on the hematite surface, the isotherms (Fig. 4c) have the shape of straight lines emanating from one point. These isotherms can be described by the Henry equation. The CO chemisorption magnitude significantly increases with increasing temperature. In the case of nanosized iron oxide, the isotherms can be classified as type I Langmuir isotherms (Fig. 4d). Noteworthy is the fact that, in the case of nanosized iron oxide, the CO

chemisorption magnitude slightly changes with increasing temperature, as evidenced by Fig. 5b.

Isosteric enthalpies of chemisorption for the studied chemisorption processes were calculated using the van't Hoff equation (Table 2).

The CO chemisorption magnitude on the nano-Fe_2O_3 surface is extremely low (-12.4 kJ/mol). These energy values are characteristic of physical sorption; this finding suggests that the interaction between the CO molecule and the nanoparticle surface is extremely weak. This feature should be taken into

Table 1. Data for Arrhenius dependences and the determination of activation energies of the reduction of nano-Fe_2O_3 and hematite

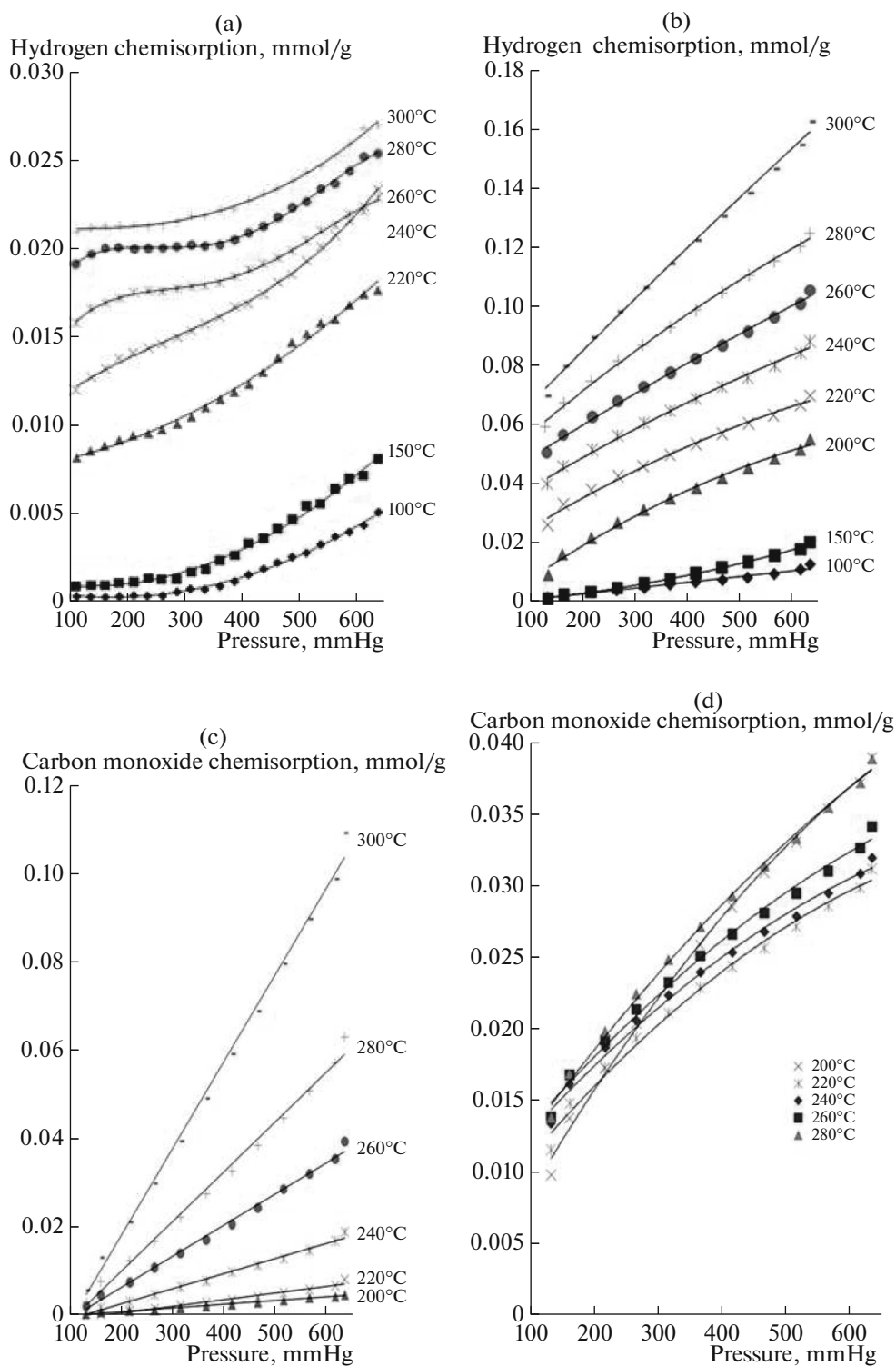| b, K/s	T_{max}, K	$10^3/T_{max}$, K^{-1}	$-\ln(b/T_{max}^2)$	b, K/s	T_{max}, K	$10^3/T_{max}$, K^{-1}	$-\ln(b/T_{max}^2)$
Nano-Fe_2O_3				Hematite Fe_2O_3			
Nano-$Fe_2O_3 \rightarrow Fe_3O_4$, $E_a = 395$ kJ/mol				$Fe_2O_3 \rightarrow Fe_3O_4$, $E_a = 73$ kJ/mol			
0.05	657	1.522	15.971	0.05	584	1.712	15.736
0.10	662	1.510	15.293	0.10	607	1.647	15.120
0.15	667	1.499	14.903	0.15	622	1.607	14.763
0.20	669	1.495	14.621	0.20	636	1.572	14.520
$Fe_3O_4 \rightarrow Fe_{1-x}O$, $E_a = 228$ kJ/mol				$Fe_3O_4 \rightarrow Fe$, $E_a = 50$ kJ/mol			
0.05	866	1.155	16.524	0.05	747	1.339	16.228
0.10	887	1.127	15.879	0.10	804	1.244	15.682
0.15	898	1.113	15.498	0.15	845	1.183	15.376
0.20	901	1.110	15.217	0.20	860	1.163	15.124
$Fe_{1-x}O \rightarrow Fe$, $E_a = 338$ kJ/mol							
0.05	675	949	1.054				
0.10	692	966	1.035				
0.15	698	972	1.029				

Fig. 4. Chemisorption isotherms of hydrogen on (a) Fe_2O_3 and (b) nano-Fe_2O_3 and carbon monoxide on (c) Fe_2O_3 and (d) nano-Fe_2O_3.

account for studying the catalytic properties of nanosized iron oxide, particularly for the selection of synthesis gas composition.

Thus, nanosized iron(III) oxide with an average particle size of 8−10 nm has been synthesized. Features of the reduction of nano-Fe_2O_3 have been stud-
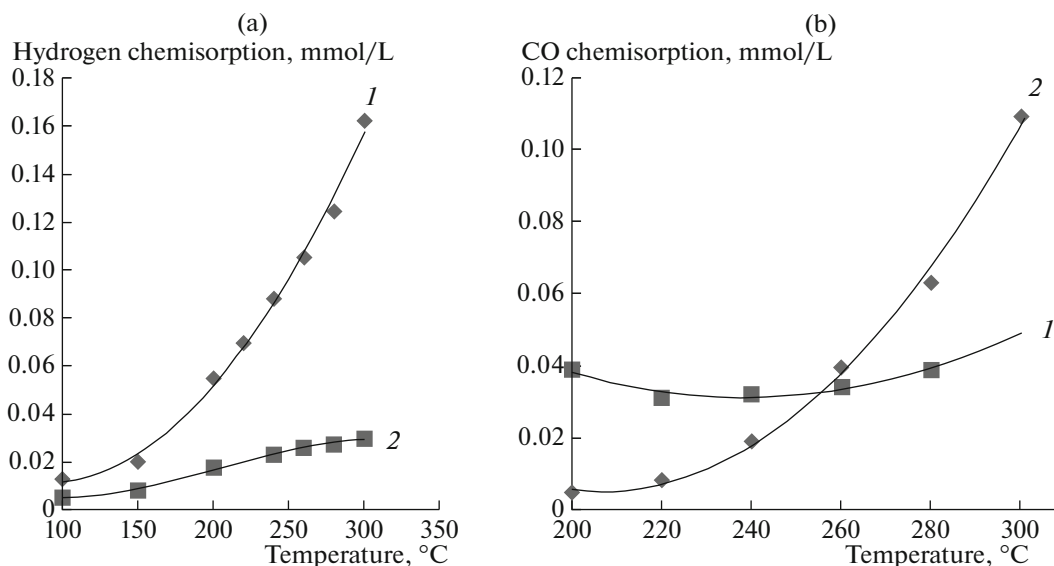
Fig. 5. Chemisorption isobars on the surface of (*1*) nano-Fe_2O_3 and (*2*) hematite at 625 mmHg: (a) hydrogen and (b) carbon monoxide.

ied by TPR. It has been shown that the reduction processes occurring in nanosized iron(III) oxide and hematite, which have the same chemical composition yet different morphology and phase composition, differ significantly. Features of the chemisorption of hydrogen and carbon monoxide on the surface of hematite and nano-Fe_2O_3 have been studied; it has been shown that the processes crucially differ and the difference is attributed to the nature of the sample, which should be taken into account in catalytic studies.

Table 2. Isosteric enthalpies of chemisorption of hydrogen and carbon monoxide on the surface of hematite and nano-Fe_2O_3

Sample	$\Delta H_{chemosorp.\ H_2}$, kJ/mol	$\Delta H_{chemosorp.\ CO}$, kJ/mol
Hematite	−35.5	−48.5
Nano-Fe_2O_3	−50.7	−12.4

REFERENCES

1. Hasany, S.F., Abdurahman, N.H., Sunarti, A.R., and Jose, R., *Curr. Nanosci.*, 2013, vol. **9**, p. 561.

2. Gupta, A.K. and Gupta, M., *Biomaterials*, 2005, vol. **26**, no. 18, p. 3995.

3. Khadzhiev, S.N. and Krylova, A.Yu., *Pet. Chem.*, 2011, vol. **51**, no. 2, p. 74.

4. Khadzhiev, S.N., Lyadov, A.S., Krylova, M.V., and Krylova, A.Yu., *Pet. Chem.*, 2011, vol. **51**, no. 1, p. 24.

5. Khadzhiev, S.N., Krylova, A.Yu., Lyadov, A.S., and Kulikova, M.V., *Pet. Chem.*, 2012, vol. **52**, no. 4, p. 240.

6. Poura, A.N., Housaindokhta, M.R., Shahrid, S.M.K., Babakhani, E.G., and Irani, M., *J. Ind. Eng. Chem.*, 2011, vol. **17**, no. 3, p. 596.

7. Fernelius, W.C., *Inorg. Synth.*, 1946, vol. **2**, p. 27.

8. Kissinger, H.E., *Anal. Chem.*, 1957, vol. **29**, no. 11, p. 1702.

9. Jozwiak, W.K., Kaczmarek, E., Maniecki, T.P., Ignaczak, W., and Maniukiewicz, W., *Appl. Catal., A*, 2007, vol. 326, p. 17.

10. Krylova, A.Yu., Chernavskii, P.A., Lyadov, A.S., Sagitov, S.A., Krylova, M.V., and Khadzhiev, S.N., *Russ. J. Phys. Chem. A*, 2011, vol. **85**, no. 1, p. 55.

Translated by M. Timoshinina